Arch. Pharm. Chem. Life Sci. 2017, *350*, e1700096

ARCH PHARM
Archiv der Pharmazie

Full Paper

Isophthalic Acid-Based HDAC Inhibitors as Potent Inhibitors of HDAC8 from *Schistosoma mansoni*

Katharina Stenzel[1], Alokta Chakrabarti[2], Jelena Melesina[3], Finn K. Hansen[1,4], Julien Lancelot[5], Simon Herkenhöhner[1], Beate Lungerich[1], Martin Marek[6], Christophe Romier[6], Raymond. J. Pierce[5], Wolfgang Sippl[3], Manfred Jung[2], and Thomas Kurz[1]

[1] Institute of Pharmaceutical and Medicinal Chemistry, Heinrich-Heine-University, Düsseldorf, Germany
[2] Institute of Pharmaceutical Sciences, Albert-Ludwigs-University Freiburg, Freiburg, Germany
[3] Institute of Pharmacy, Martin-Luther-University Halle-Wittenberg, Halle (Saale), Germany
[4] Pharmaceutical/Medicinal Chemistry, Institute of Pharmacy, Leipzig University, Leipzig, Germany
[5] Univ. Lille, CNRS, Inserm, CHU Lille, Institut Pasteur de Lille, U1019 UMR 8204CIIL – Centre d'Infection et d'Immunité de Lille, Lille, France
[6] IGBMC, Université de Strasbourg, Illkirch, France

Schistosoma mansoni histone deacetylase 8 (*Sm*HDAC8) has been recently identified as a new potential target for the treatment of schistosomiasis. A series of newly designed and synthesized alkoxyamide-based and hydrazide-based HDAC inhibitors were tested for inhibitory activity against *Sm*HDAC8 and human HDACs 1, 6, and 8. The front runner compounds showed submicromolar activity against *Sm*HDAC8 and modest preference for *Sm*HDAC8 over its human orthologue hHDAC8. Docking studies provided insights into the putative binding mode in *Sm*HDAC8 and allowed rationalization of the observed selectivity profile.

Keywords: Docking studies / HDAC8 / Histone deacetylase inhibitors / *Schistosoma mansoni* / Schistosomiasis

Received: March 16, 2017; Revised: May 21, 2017; Accepted: May 22, 2017

DOI 10.1002/ardp.201700096

Additional supporting information may be found in the online version of this article at the publisher's web-site.

Introduction

The neglected parasitic disease schistosomiasis is endemic in 74 developing countries. The disease continues to spread to new geographic areas despite comprehensive anthelmintic drug therapy programs. There are two major forms of schistosomiasis – intestinal and urogenital – caused by *Schistosoma mansoni* and four further parasites of the genus *Schistosoma* that infect humans. Chronic disease contributes to major organ damage, and reducing the severity of symptoms is critical to the management of schistosomiasis. Under risk are individuals having contact with freshwater sources and in particular children under age 14. According to World Health Organization (WHO) statistics at least 258 million people worldwide required preventive treatment and 62 million received treatment in 2014 [1, 2].

The life cycle of *S. mansoni* includes radical morphological modifications and exhibits diverse phenotypes [3, 4]. The complexity of the human endoparasite is reflected in a large genome, variable transcriptome profiles, and a dynamic epigenetic machinery in dependency of each life cycle stage [5, 6]. There is currently no vaccine available for the treatment of human schistosomiasis and no indication that a vaccine is likely to become available soon [7].

Since the anthelminthic drug praziquantel (PZQ) was approved for treatment of schistosomiasis it has been widely used for more than 30 years and remains to be the drug of choice till now [8]. The WHO strategy for schistosomiasis

Correspondence: Prof. Thomas Kurz, Institut für Pharmazeutische und Medizinische Chemie, Heinrich-Heine-Universität Düsseldorf, Universitätsstr. 1, 40225 Düsseldorf, Germany.
E-mail: thomas.kurz@uni-duesseldorf.de
Fax: +49 211 81-13847

control focuses on periodic large scale treatment with PZQ (preventive chemotherapy) of affected populations. However, the drug does not prevent reinfections and its mechanism of action is not exactly known. The application of PZQ is limited to adult worms, which has been shown in *in vitro* tests and confirmed by clinical data [9, 10]. PZQ is safe, effective and relatively cheap, but there is also a growing concern regarding reports from patients not cured by multiple doses [11, 12]. The development of resistance and stable resistance after removal of drug pressure has been demonstrated in the laboratory [13–15]. Moreover resistant isolates have already been characterized in endemic areas and the selection of field strains of schistosome that are resistant to PZQ is more and more likely [9].

Like other human parasites schistosomes share some properties with malignant tumors including intense metabolic activity and uncontrolled cell division [16–18]. Histone deacetylases (HDACs) are Zn^{2+}- or NAD^{+}-dependent lysine deacetylases that can modulate cell chromatin structure, transcription, and gene expression. Consequently, histone deacetylase inhibitors (HDACi) have emerged as a new class of anticancer drugs. Currently, three HDACi are approved by the US Food and Drug Administration (FDA) for the treatment of T-cell lymphoma (vorinostat, romidepsin, and belinostat) while panobinostat has been approved for combination therapy use in certain cases of multiple myeloma. Furthermore, the potential therapeutic use of HDACi in other diseases including inflammatory, immune, neurodegenerative, cardiac, viral, and parasitic diseases is currently under discussion [19–27].

Using the "piggyback" strategy it has been shown that the HDACi trichostatin A (TSA), vorinostat (SAHA), and valproic acid (VPA) inhibited *S. mansoni* histone deacetylase 8 (*Sm*HDAC8) activity at all life cycle stages and TSA and VPA caused mortality of schistosomula and adult worms [25, 28, 29]. Till now only class I *S. mansoni* HDAC1, -3, and -8 and class III *S. mansoni* Sirt1, -2, -5, -6, -7 HDACs have been cloned and characterized [29, 30]. *S. mansoni* HDAC1, 3, and 8 mRNAs are expressed at all schistosome life cycle stages. In particular, *Sm*HDAC8 has been identified as a potential target for antiparasitic therapy [31]. Transcripts of *Sm*HDAC8 are expressed at higher levels than *Sm*HDAC1 and *Sm*HDAC3 during all life cycle stages, pointing at specific and vital functions in the parasite life cycle. At the same time human HDAC8 shows the lowest level of expression of the four class I HDACs in human and it has been reported that inhibition of hHDAC8 shows only limited effects in many cell types [32]. Different HDACi have already been shown to inhibit *Sm*HDAC8 and to induce histone hyperacetylation and apoptosis in *S. mansoni* [29, 31, 33].

Treatment of schistosomes with HDACi caused an accumulation of acetylated cellular proteins and dose-dependent mortality of schistosomula and adult worms [6, 28, 29]. Thus, the development of small-molecule *Sm*HDAC8 inhibitors represents a promising approach for the treatment of schistosomiasis and several HDACi with confirmed activity against *Sm*HDAC8 have been identified in recent years (see Fig. 1 for selected examples) [32, 34]. Unfortunately, most known *Sm*HDAC8 inhibitors possess a higher activity against human HDAC8. Thus, there is a strong need for new types of HDACi with preferential activity for *Sm*HDAC8. We herein present the design, synthesis, and biological evaluation of a novel series of *Sm*HDAC8 inhibitors.

Results and discussion

Design and synthesis of target compounds

We used the 3-acylaminobenzohydraxamates of type **I** and **II** (Fig. 1), a series of potent and in some cases preferential *Sm*HDAC8 inhibitors, as starting point for this project [34]. In a previous study [21, 35] we identified an alkoxyamide group as a novel connecting unit which presumably can enable charge-assisted hydrogen bonds due to the additional polarization of the N–H bond. We therefore decided to retain the *meta*-substituted benzohydroxamate realized in **I** and to combine this motif with an alkoxyamide connecting unit and various cap groups. In addition, we designed compounds with hydrazide-based connecting units in order to probe whether these groups can serve as an alternative connecting unit.

The isophthalic acid-based target compounds **3a–i** and **5a,b** were synthesized using a straightforward two-step protocol as illustrated in Scheme 1. First, the 1,1′-carbonyldiimidazole (CDI)-mediated amide coupling reaction of mono-methyl isophthalate with *O*-substituted hydroxylamines and hydrazine derivatives provided the alkoxyamide intermediates **2a–i** and hydrazides **4a,b** (Scheme 1), respectively.

The subsequent treatment of **2a–i** and **4a,b** with an excess of hydroxylamine hydrochloride in the presence of methanolic sodium methoxide afforded the desired target compounds **3a–i** and **5a,b**. Using these synthetic methods allowed us to efficiently modify the cap region of our target compounds in order to potentially address the hydrophobic side pocket of *Sm*HDAC8.

Primary screening

All synthesized compounds were first tested in a primary screen for inhibition of *Sm*HDAC8 and representative human HDAC isoforms (hHDAC1, hHDAC6, and hHDAC8) at a concentration of 1 μM (Table 1). The *in vitro* assays rely on the use of fluorogenic substrates containing an ε-acetyl lysine linked to a fluorescent moiety at the C-terminus. Only upon deacetylation the resulting peptide is a substrate for a protease which upon cleavage of the fluorogenic moiety releases the fluorophore for quantitation. For HDAC1 and 6 we used ZMAL (Z-Lys(Ac)-AMC) and trypsin as the protease. The commercially available Fluor de Lys-HDAC8 substrate has Arg-His-Lys(Ac)-Lys(Ac) as the substrate sequence. The exact identity of fluorophore and developer are not revealed [36, 37]. All compounds showed significant inhibition of *Sm*HDAC8 deacetylase activity, moderate inhibition of hHDAC6 and only very low inhibition of hHDAC1. However,

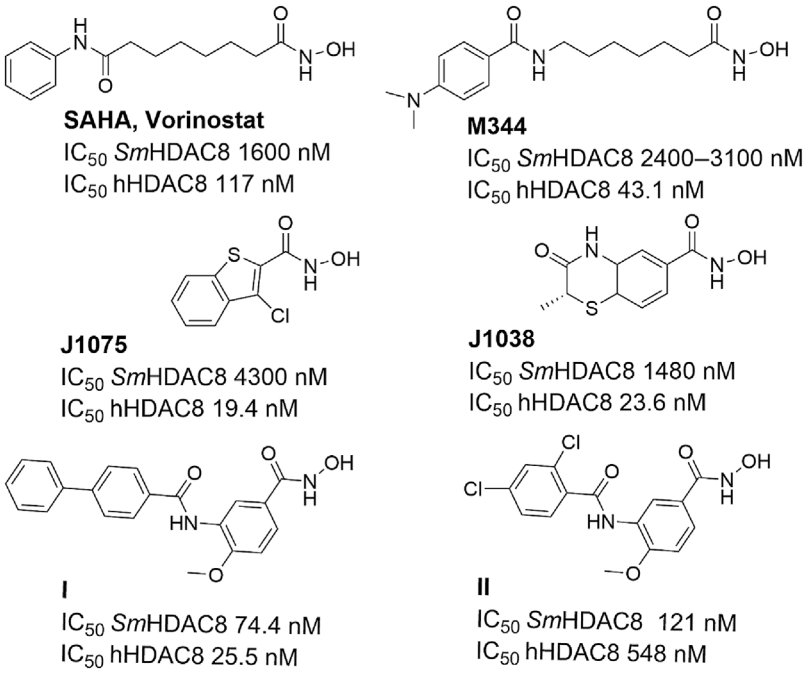

Figure 1. Chemical structures of selected HDAC inhibitors and IC_{50} values of *Sm*HDAC8 and hHDAC8 [22, 24].

most compounds inhibited hHDAC8 in similar fashion as *Sm*HDAC8. Interestingly, compounds **3d** and **5a** revealed a somewhat stronger inhibition of *Sm*HDAC8 in comparison to hHDAC8 (Table 1). Based on this primary screening, we decided to investigate the HDACi **3d**, **5a** and the unsubstituted prototype compound **3c** in more detail.

Inhibition of hHDAC1, hHDAC6, hHDAC8, and *Sm*HDAC8

In order to study whether **3c**, **3d**, and **5a** can be considered as preferential *Sm*HDAC8 inhibitors, we determined IC_{50} values against hHDAC1, hHDAC6, hHDAC8, and *Sm*HDAC8. SAHA (vorinostat, suberoylanilide hydroxamic acid) was used as a reference pan-HDACi. The results are summarized in Table 2. Compounds **3c**, **3d**, and **5a** showed nanomolar activity against *Sm*HDAC8 with IC_{50} values in the range of 0.33–0.75 μM and very good selectivity over hHDAC1. Furthermore, the compounds possess approximately 10-fold preference over hHDAC6. The compound **3c** exhibited a stronger inhibition of hHDAC8 (IC_{50}: 0.09 μM) compared with *Sm*HDAC8 (IC_{50}: 0.33 μM) whereas **3d** (hHDAC8 IC_{50}: 0.63 μM vs. *Sm*HDAC8 IC_{50}: 0.40 μM) and **5a** (hHDAC8IC_{50}: 1.31 μM vs. *Sm*HDAC8 IC_{50}: 0.75 μM) showed a very modest preference for *Sm*HDAC8.

Docking study

To rationalize the obtained biochemical data, notably to understand the change of specificity between the schistosomal and human enzymes, the synthesized inhibitors were docked to the available crystal structures of *Sm*HDAC8, hHDAC8, and hHDAC1. The applied docking method was first successfully validated on the X-ray structures of hHDAC8 and *Sm*HDAC8 (for details see the Experimental section). Using this docking setup consistent binding models were derived for both human and *Sm*HDAC8. Comparison of the available X-ray structures of hHDAC8 and *Sm*HDAC8 showed a

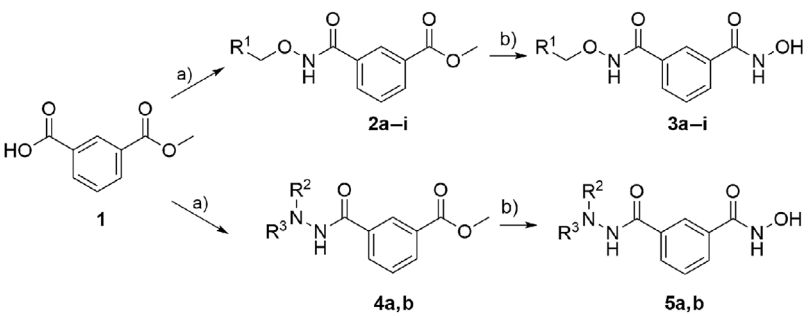

Scheme 1. Synthesis of alkoxyamide-based and the hydrazide-based HDACi. Reagents and conditions: a) CDI, CH_2Cl_2, R^1-ONH_2, or R^1R^2-NNH_2, r.t., 0.5 h, 12 h; b) 1) NaOMe, MeOH, $NH_2OH{\cdot}HCl$, 70°C, 3–5 h, 2) NaOH, NH_2OH, MeOH, CH_2Cl_2, 0°C, r.t., 12 h.

Table 1. % Inhibition of hHDAC1, hHDAC6, hHDAC8, and *Sm*HDAC8 at 1 μM.

		% Inhibition at 1 μM: Primary screen				
		R^1	hHDAC1	hHDAC6	hHDAC8	*Sm*HDAC8
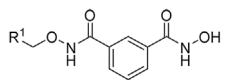 3a–i	**3a**	Ph-CH_2-CH_2	<10	65	81	87
	3b	Ph-CH_2	<10	43	63	84
	3c	Ph	<10	31	79	89
	3d	2,4-Cl-Ph	<10	20	56	86
	3e	2,3-Cl-Ph	<10	52	76	90
	3f	3,5-Me-Ph	<10	41	73	78
	3g	4-Me-Ph	<10	50	88	90
	3h	1-naphthyl	<10	51	78	84
	3i	3,4-F-Ph	<10	41	72	82
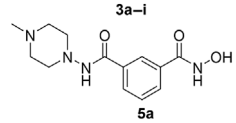 5a	**5a**		<10	26	38	64
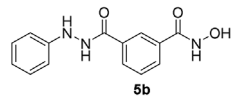 5b	**5b**		<10	49	70	87

high similarity especially within the binding pocket. The main differences are the subsitution of Met274 in hHDAC8 to His292 in *Sm*HDAC8 and a flipped out conformation of Phe151 in *Sm*HDAC8 (for details see Fig. S1a and b in the Supporting Information). Docking of inhibitors **3c**, **3d**, and **5a** to *Sm*HDAC8 and hHDAC8 showed that the hydroxamate is perfectly coordinating the zinc ion as observed in *Sm*/hHDAC8-inhibitor crystal structures. In addition the hydroxamate group is making hydrogen bonds to conserved Tyr and His residues nearby the catalytic zinc ion (see Fig. 2A–C for details). Docking of **3c** and **3d,** having an alkoxyamide linker between the two aromatic rings, showed in case of *Sm*HDAC8 two additional hydrogen bonds to Lys20 and His292 (Fig. 2A, B). These interactions are also observed in the crystal structure of *Sm*HDAC8 in complex with an amide containing inhibitor (PDB ID 5FUE) [34]. Only compounds **3c** and **3d** are showing these two hydrogen bonds, whereas the weaker *Sm*HDAC8 inhibitor **5a** is not able to form these hydrogen bonds but interacts with Asp100. Additionally, the calculated binding energies of **3c** and **3d** are more favourable compared to **5a** (see Supporting Information Table S1). The terminal aromatic group of **3c** and **3d** is interacting with the residues of the so-called side-pocket (His292, Pro293, Tyr306). The docking of **5a** showed that the piperazine ring is located nearby the acidic residue Asp100 (hydrogen bond in case of *Sm*HDAC8) whereas no interaction with the residues of the side-pocket was observed, which might explain the lower inhibitory activity.

In the hHDAC8 structure a methionine (Met274) is located at the same position as His292 in *Sm*HDAC8. The methionine is not able to form hydrogen bonds with the docked inhibitors. However, in the available crystal structures of hHDAC8 a conserved water molecule bound to the zinc coordinating histidine (His180 in hHDAC8) is observed which was found as a hydrogen bonding partner with **3c** and **3d** (Fig. 2D,E). The terminal aromatic ring of **3c** makes favorable van der Waals interaction with the side-pocket in hHDAC8 (Phe152, Pro273, Met274, Tyr341, Fig. 2) and shows a perfect fit to this hydrophobic subpocket (Fig. 3). This is reflected by favourable docking score and binding energy calculated for **3c** (Supporting Information Table S1). The docking of the

Table 2. IC_{50} profiling against human hHDAC1, hHDAC6, hHDAC8, and *Sm*HDAC8.

		IC_{50} (μM)			
		hHDAC1	hHDAC6	hHDAC8	*Sm*HDAC8
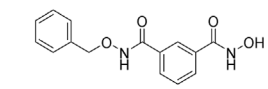 3c	**3c**	136.1	2.95	0.09 ± 0.12	0.33 ± 0.04
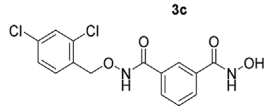 3d	**3d**	47.5% @200 μM	5.12	0.63 ± 0.14	0.40 ± 0.078
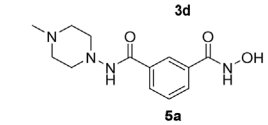 5a	**5a**	15.3% @200 μM	7.11	1.31 ± 0.13	0.75 ± 0.22
	SAHA	0.32	0.11	0.91 ± 0.26	1.38 ± 0.70

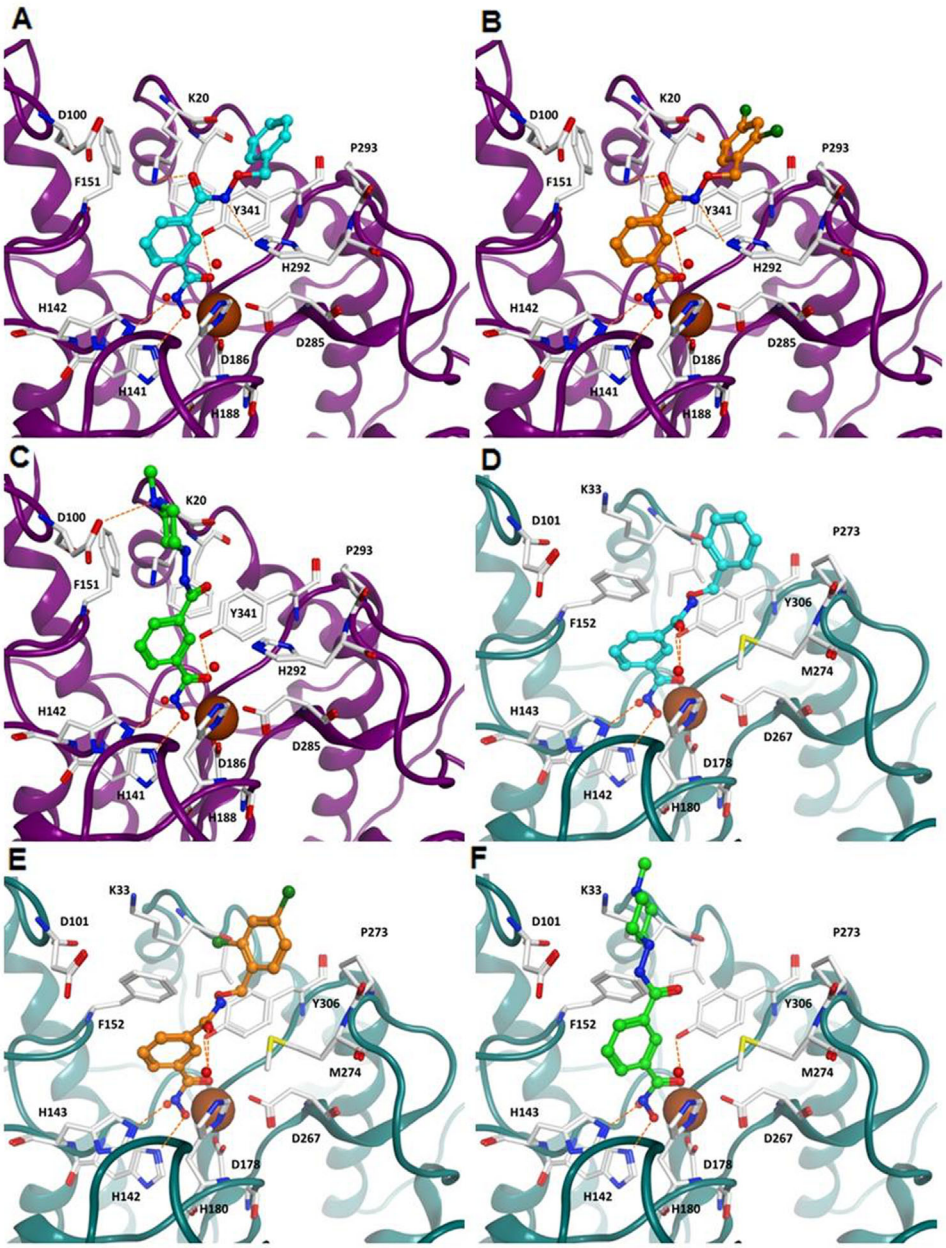

Figure 2. Docking poses calculated for inhibitor **3c** (colored cyan), **3d** (colored orange), and **5a** (colored green) at *Sm*HDAC8 (purple ribbon) and at hHDAC8 (turquoise ribbon). Only surrounding amino acid residues are shown for clarity. Hydrogen bonds are shown as orange dashed lines.

inhibitors to hHDAC1 showed that the hydroxamate is not able to coordinate in a favorable manner to the catalytic zinc ion due to a narrower binding pocket (Fig. 4).

Cytotoxicity and phenotypic activity

Parasite-specific HDACi should possess low toxicity to mammalian cells. We therefore tested **3d** and **5a** for cytotoxicity against HeK293T and HeLa cells. Vorinostat was used as reference compound. The results are summarized in Fig. 5. As expected, vorinostat exhibited strong cytotoxicity against both HeK293T and HeLa cells. In contrast, compounds **3d** and **5a** showed only relatively low cytotoxicity (Fig. 5).

We next studied the phenotypic activity of **3d** and **5a** by testing their effects on the viability of the larvae (schistosomula) and the stability of adult worm pairs in culture exactly as

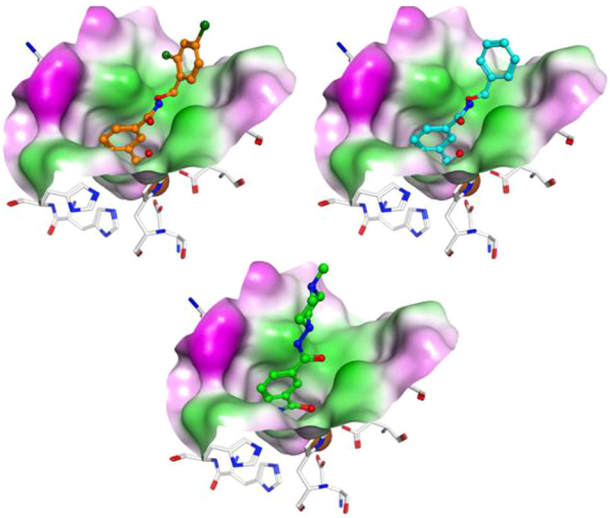

Figure 3. Molecular surface of the hHDAC8 binding pocket colored according to the hydrophobicity (green = hydrophobic, magenta = hydrophilic). The docking pose of inhibitor **3c** is shown in cyan, **3d** is shown in orange, and **5a** is shown in green.

previously described [34]. Using a fluorescence-based assay **3d** showed moderate toxicity toward schistosomula at 10 μM, but this was not dose-dependent. **5a** showed only slight activity. Moreover, neither compound significantly affected adult worm pairing during 5 days of culture *in vitro* (Table 3). Of note, vorinostat is only moderately effective in the same assays (not shown), whereas other hydroxamate-based inhibitors are very active [29, 34]. The different abilities of the compounds to pass through the parasite tegument may provide a possible explanation for these differences.

Conclusion

In summary, we have designed and synthesized two new types of isophthalic acid-based *Sm*HDAC8 inhibitors. The alkoxyamide-based HDACi **3d** and the hydrazide-based HDACi **5a** were identified as potent inhibitors of *Sm*HDAC8 with a high preference over hHDAC1 and good preference over hHDAC6. Cytotoxicity studies revealed that the compounds showed relatively low effects on the proliferation of human cells. Molecular modeling and docking studies allowed rationalization of the observed biochemical data and suggest that two important hydrogen bonds of the alkoxyamide connecting unit to Lys20 and His292 contribute to the high activity of **3d** against *Sm*HDAC8. Even though the preference over hHDAC8 and the phenotypic activity need to be improved in the future, we believe that **3d** and **5a** are valuable starting points for the development of novel preferential *Sm*HDAC8 inhibitors.

Experimental

Chemistry

*General procedure for the synthesis of **3a–i** and **5a,b***

Method A: Hydroxylamine hydrochloride (348 mg, 5.0 mmol, 10 eq) was added to a freshly prepared sodium methanolate solution (175 mg, 7.5 mmol, 15 eq) in dry methanol (8 mL). The mixture was stirred for 10 min before the respective ester **2a–i** or **4a** (0.5 mmol, 1.0 eq) was added. The reaction mixture was stirred in a high-pressure flask for 3–5 h at 70°C. The solvent was removed under reduced pressure, water (15 mL) was added, and the pH was adjusted to pH 7–8 using 4 M HCl. The mixture was extracted with ethyl acetate (3 × 20 mL), the combined organic layers were dried over anhydrous sodium sulfate, filtered, and concentrated in vacuum. The crude products were purified by flash column chromatography using a linear dichloromethane/methanol gradient (pre-packed silica cartridge, gradient: 97:3 to 91:9 in 20 min) to yield the desired hydroxamic acids **3a–i** and **5a–b** (yield: 60–91%). Method B: The respective ester **4b** (1 mmol, 1.0 eq) was dissolved in dry dichlormethane/methanol (1:3) and cooled down to 0°C. Hydroxylamine (50 wt% in water, 30 mmol, 30 eq) and NaOH (0.4 g, 10 mmol, 10 eq) were added and stirred for 12 h at room temperature. The solvent was removed under reduced pressure, water (15 mL) was added, and the pH was adjusted to pH 7–8 using 4 M HCl. The mixture was extracted with ethyl acetate (3 × 20 mL), the combined organic layers were dried over anhydrous sodium sulfate, filtered, and concentrated in vacuum (yield: 86%).

The InChI codes of the investigated compounds together with some biological activity data are provided as Supporting Information.

*N^1-Hydroxy-N^3-(3-phenylpropoxy)isophthalamide (**3a**)*

Colorless solid; yield: 84%; mp: 130°C; ^{1}H NMR (600 MHz, DMSO-d_6) δ 10.69 (s, 2H), 8.18 (s, 1H), 7.84–7.94 (m, 2H), 7.55 (t, J = 7.1 Hz, 1H), 7.42–7.22 (m, 4H), 7.22–7.07 (m, 1H), 3.92 (s, 2H), 2.73 (s, 2H), 1.92 (s, 2H). ^{13}C NMR (151 MHz, DMSO) δ 162.95, 162.90, 141.01, 132.53, 132.07, 129.04, 128.96, 128.01, 127.79, 127.72, 125.32, 125.20, 73.96, 30.85, 29.05. t_R: 11.68 min, purity: 97.2%; HRMS (ESI) Anal. calcd. for $C_{17}H_{19}N_2O_4$ 315.1345 $[M+H]^+$, Found 315.1342.

*N^1-Hydroxy-N^3-phenethoxyisophthalamide (**3b**)*

Colorless solid; yield: 78%; mp: 128°C; ^{1}H NMR (500 MHz, DMSO-d_6) δ 11.55 (s, 2H), 9.18 (s, 1H), 8.16 (s, 1H), 7.88 (t, J = 8.1 Hz, 2H), 7.55 (t, J = 7.7 Hz, 1H), 7.42–7.27 (m, 4H), 7.27–7.11 (m, 1H), 4.13 (t, J = 6.9 Hz, 2H), 2.97 (t, J = 6.9 Hz, 2H). ^{13}C NMR (126 MHz, DMSO) δ 163.43, 138.27, 133.00, 132.49, 129.58, 129.48, 128.78, 128.51, 128.20, 126.09, 125.86, 75.64, 33.93. t_R: 10.65 min, purity: 97.5%; HRMS (ESI) Anal. calcd. for $C_{16}H_{17}N_2O_4$ 301.1188 $[M+H]^+$, Found 301.1182.

*N^1-(Benzyloxy)-N^3-hydroxyisophthalamide (**3c**)*

Colorless solid; yield: 60%; mp: 159°C; ^{1}H NMR (500 MHz, DMSO-d_6) δ 11.92 (s, 1H), 11.34 (s, 1H), 9.14 (s, 1H), 8.16 (s, 1H),

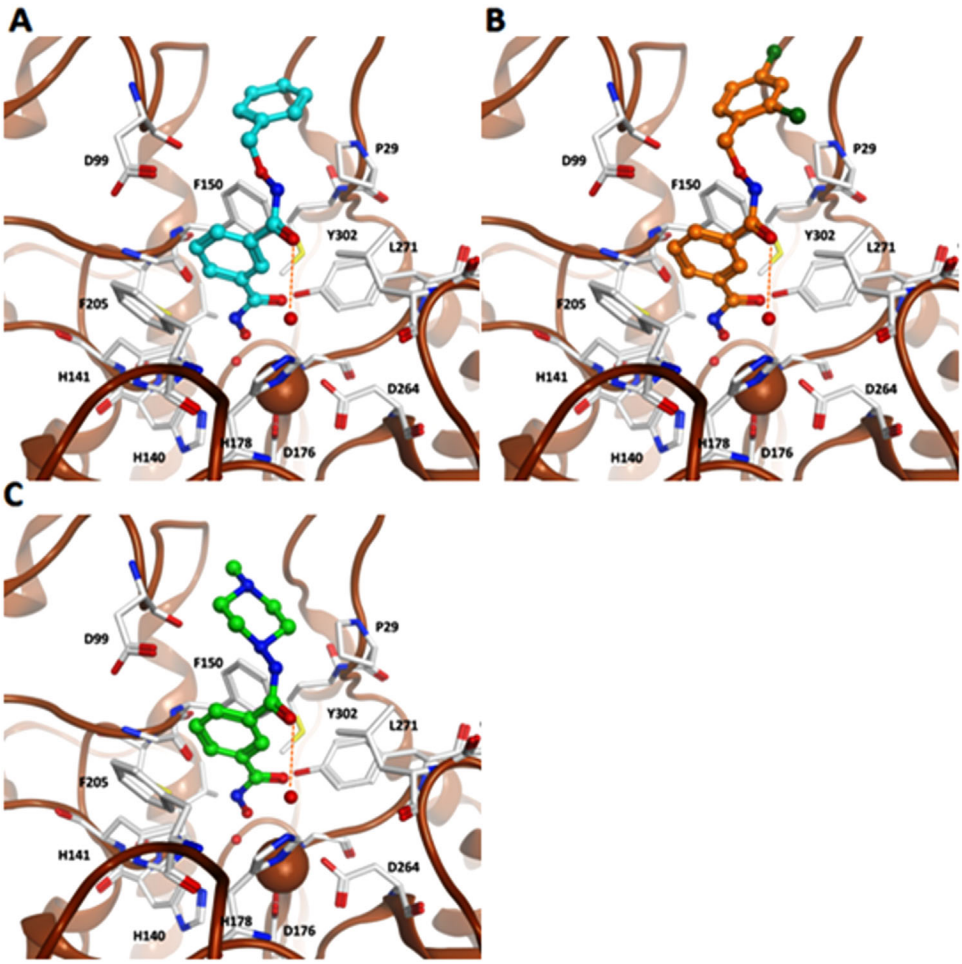

Figure 4. Docking poses calculated for inhibitor **3c** (colored cyan), **3d** (colored orange), and **5a** (colored green) at hHDAC1. Only surrounding amino acid residues are shown for clarity. Hydrogen bonds are shown as orange dashed lines.

8.05–7.75 (m, 2H), 7.62–7.26 (m, 6H), 4.94 (s, 2H). ^{13}C NMR (126 MHz, DMSO) δ 163.72, 163.46, 135.76, 132.98, 132.45, 129.62, 129.51, 128.82, 128.52, 128.23, 125.91, 76.93. t_R: 9.62 min, purity: 97.2%; HRMS (ESI) Anal. calcd. for $C_{15}H_{15}N_2O_4$ 287.1032 $[M+H]^+$, Found 287.1024.

*N^1-((2,4-Dichlorobenzyl)oxy)-N^3-hydroxyisophthalamide (**3d**)*
Colorless solid; yield 82%; mp: 130°C; ^{1}H NMR (600 MHz, DMSO-d_6) δ 11.51 (s, 2H), 9.43 (s, 1H), 8.14 (s, 1H), 7.88 (d, J = 7.7 Hz, 1H), 7.84 (d, J = 7.6 Hz, 1H), 7.67 (s, 1H), 7.64 (d, J = 8.2 Hz, 1H), 7.53 (t, J = 7.7 Hz, 1H), 7.49 (dd, J = 8.3,

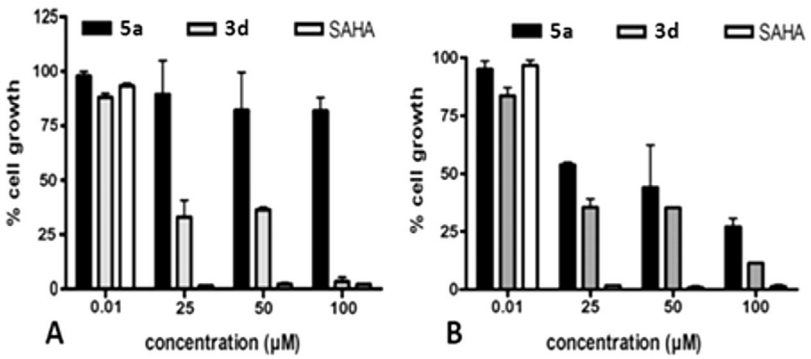

Figure 5. Comparison of cell viability of **3d** and **5a** in human cell lines. HeK293(A) and HeLa(B) cell lines were treated with the indicated concentrations of inhibitors for 72 h. Cell viability was measured using the 3-(4,5-dimethylthiazol-2-yl)-5-(3-carboxymethoxyphenyl)-2-(4-sulfo-phenyl)-2*H*-tetrazolium/phenazine methosulfate (MTS/PMS) reagent. Data represent S.E. of the mean (duplicates).

ARCH PHARM
Archiv der Pharmazie

Table 3. Toxicity studies on *S. mansoni* adult worms and schistosomula.

Compound	% Pairing ± SEM	% Viability ± SD
3d		
10 μM	95 ± 5	76 ± 6
20 μM	85 ± 5	75 ± 4
5a		
10 μM	95 ± 5	90 ± 9
20 μM	95 ± 5	79 ± 3

Experimental conditions: Single dose at $D = 0$, duration: 3 days data represent the means of three independent experiments. Adult worm pairing assay: Number of worms: 10/wells $n = 2$ Alamar viability assay: Number of schistosomula: 100/well $n = 2$.

2.2 Hz, 1H), 5.04 (s, 2H). ^{13}C NMR (151 MHz, DMSO) δ 163.12, 162.91, 133.63, 133.24, 132.47, 132.28, 132.03, 131.86, 129.11, 129.03, 128.20, 128.01, 126.83, 125.40, 72.46. t_R: 12.40 min, purity: 99.1%; HRMS (ESI) Anal. calcd. for $C_{15}H_{13}Cl_2N_2O_4$ 355.0252 $[M+H]^+$, Found 355.0244.

*N^1-((2,3-Dichlorobenzyl)oxy)-N^3-hydroxyisophthalamide (**3e**)*
Colorless solid; yield 91%; mp: 116°C; ^{1}H NMR (600 MHz, DMSO-d_6) δ 11.75 (s, 1H), 11.47 (s, 1H), 9.13 (s, 1H), 8.13 (s, 1H), 7.89 (d, $J = 7.6$ Hz, 1H), 7.84 (d, $J = 7.7$ Hz, 1H), 7.67 (d, $J = 7.9$ Hz, 1H), 7.60 (d, $J = 7.5$ Hz, 1H), 7.55 (t, $J = 7.7$ Hz, 1H), 7.42 (t, $J = 7.8$ Hz, 1H), 5.11 (s, 2H). ^{13}C NMR (151 MHz, DMSO) δ 163.52, 162.93, 135.68, 135.63, 132.50, 131.76, 131.28, 130.60, 129.91, 129.15, 129.05, 128.03, 127.60, 125.42, 73.62. t_R: 12.10 min, purity: 96.3%; HRMS (ESI) Anal. calcd. for $C_{15}H_{13}Cl_2N_2O_4$ 355.0252 $[M+H]^+$, Found 355.0247.

*N^1-((3,5-Dimethylbenzyl)oxy)-N^3-hydroxyisophthalamide (**3f**)*
Colorless solid; yield 84%; mp: 105°C; ^{1}H NMR (500 MHz, DMSO-d_6) δ 11.86 (s, 1H), 11.33 (s, 1H), 9.14 (s, 1H), 8.16 (s, 1H), 7.94–7.83 (m, 2H), 7.56 (t, $J = 7.7$ Hz, 1H), 7.07 (s, 2H), 7.00 (s, 1H), 4.86 (s, 2H), 2.29 (s, 6H). ^{13}C NMR (126 MHz, DMSO-d_6) ^{13}C NMR (151 MHz, DMSO) δ 164.30, 164.06, 137.78, 136.13, 133.57, 133.12, 130.15, 129.10, 127.15, 126.51, 77.59, 21.32. t_R: 12.03 min, purity: 97.5%; HRMS (ESI) Anal. calcd. for $C_{17}H_{19}N_2O_4$ 315.1345 $[M+H]^+$, Found 315.1343.

*N^1-Hydroxy-N^3-((4-methylbenzyl)oxy)isophthalamide (**3g**)*
Colorless solid; yield 78%; mp: 169°C; ^{1}H NMR (600 MHz, DMSO-d_6) δ 11.56 (s, 2H), 9.15 (s, 1H), 8.15 (s, 1H), 7.89 (d, $J = 7.7$ Hz, 1H), 7.86 (d, $J = 7.8$ Hz, 1H), 7.55 (t, $J = 7.7$ Hz, 1H), 7.35 (d, $J = 7.6$ Hz, 2H), 7.21 (d, $J = 7.6$ Hz, 2H), 4.89 (s, 2H), 2.32 (s, 3H). ^{13}C NMR (151 MHz, DMSO) δ 163.16, 162.95, 137.02, 132.49, 132.28, 131.98, 129.04, 128.95, 128.43, 128.28, 128.01, 125.36, 76.24, 20.22. t_R: 10.85 min, purity: 97.1%; HRMS (ESI) Anal. calcd. for $C_{16}H_{17}N_2O_4$ 301.1188 $[M+H]^+$, Found 301.1184.

*N^1-Hydroxy-N^3-(naphthalen-1-ylmethoxy)isophthalamide (**3h**)*
Colorless solid; yield: 81%; mp: 137°C; ^{1}H NMR (600 MHz, DMSO-d_6) δ 11.97 (s, 1H), 11.09 (s, 1H), 9.17 (s, 1H), 8.62 (d, $J = 8.0$ Hz, 1H), 8.22 (s, 1H), 7.98 (d, $J = 8.1$ Hz, 2H), 7.91 (t, $J = 6.5$ Hz, 2H), 7.68–7.55 (m, 4H), 7.49–7.54 (m, 1H), 5.39 (s, 2H). ^{13}C NMR (126 MHz, DMSO) δ 164.78, 164.37, 134.21, 134.09, 133.47, 132.91, 132.33, 130.59, 130.45, 130.24, 129.47, 129.36, 129.12, 127.29, 126.87, 126.15, 125.75, 76.23. t_R: 12.28 min, purity: 97.4%; HRMS (ESI) Anal. calcd. for $C_{19}H_{17}N_2O_4$ 337.1188 $[M+H]^+$, Found 337.1185.

*N^1-((3,4-Difluorobenzyl)oxy)-N^3-hydroxyisophthalamide (**3i**)*
Colorless solid; yield 73%; mp: 120°C; ^{1}H NMR (600 MHz, DMSO-d_6) δ 11.57 (s, 2H), 9.28 (s, 1H), 8.18 (s, 1H), 7.88 (d, $J = 7.5$ Hz, 1H), 7.91 (d, $J = 7.6$ Hz, 1H), 7.64–7.50 (m, 2H), 7.49–7.42 (m, 1H), 7.33 (s, 1H), 4.95 (s, 2H). ^{13}C NMR (151 MHz, DMSO) δ 163.02, 162.89, 148.71 (dd, $J = 245.4$, 10.5 Hz), 148.61 (dd, $J = 245.2$, 11.9 Hz), 133.46, 132.45, 131.82, 129.14, 129.02, 128.03, 125.37, 125.07 (dd, $J = 6.2$, 3.0 Hz), 117.11 (d, $J = 17.3$ Hz), 116.74 (d, $J = 17.1$ Hz), 74.96. t_R: 10.83 min, purity: 98.9%; HRMS (ESI) Anal. calcd. for $C_{15}H_{13}F_2N_2O_4$ 323.0843 $[M+H]^+$, Found 323.0835.

*N^1-Hydroxy-N^3-(4-methylpiperazin-1-yl)isophthalamide (**5a**)*
Colorless solid; yield: 65%; mp: 155°C; ^{1}H NMR (600 MHz, DMSO-d_6) δ 11.40 (s, 1H), 9.72 (s, 1H), 9.15 (s, 1H), 8.24 (s, 1H), 7.94–7.86 (m, 2H), 7.53 (t, $J = 7.5$ Hz, 1H), 2.97 (s, 4H), 2.66 (s, 4H), 2.33 (s, 3H). ^{13}C NMR (151 MHz, DMSO) δ 163.05, 162.98, 133.43, 132.21, 129.35, 128.88, 127.81, 125.47, 53.20, 52.32, 43.97. t_R: 4.79 min, purity: 98.1%; HRMS (ESI) Anal. calcd. for $C_{13}H_{19}N_4O_3$ 279.1457 $[M+H]^+$, Found 279.1453.

*N-Hydroxy-3-(2-phenylhydrazine-1-carbonyl)benzamide (**5b**)*
Colorless solid; yield 86%; mp: 182°C; ^{1}H NMR (600 MHz, DMSO-d_6) δ 11.34 (s, 1H), 10.44 (s, 1H), 9.14 (s, 1H), 8.29 (s, 1H), 8.04 (d, $J = 7.7$ Hz, 1H), 7.99–7.89 (m, 2H), 7.59 (t, $J = 7.7$ Hz, 1H), 7.16 (t, $J = 7.9$ Hz, 2H), 6.81 (d, $J = 7.8$ Hz, 2H), 6.73 (t, $J = 7.3$ Hz, 1H). ^{13}C NMR (151 MHz, DMSO) δ 165.33, 163.07, 148.78, 132.73, 132.56, 129.21, 129.15, 128.14, 128.06, 125.61, 118.08, 111.74. t_R: 9.59 min, purity: 98.4% HRMS (ESI) Anal. calcd. for $C_{25}H_{25}N_2O_4$ 417.1804 $[M+H]^+$, Found 417.1809. HRMS (ESI) Anal. calcd. for $C_{14}H_{14}N_3O_3$ 272.1035 $[M+H]^+$, Found 272.1032.

Biological evaluation

Phenotypic screening of schistosomes
The viability of *S. mansoni* schistosomula in the presence of *Sm*HDAC8 inhibitors was measured with a fluorescence-based assay using Alamar blue as previously described [24], as was

the effect of the compounds on the stability of adult worm pairing [24].

Computational methods

Crystal structures of *Sm*HDAC8 (PDB ID 5FUE), hHDAC8 (PDB ID 2V5X) and hHDAC1 (PDB ID 4BKX) were downloaded from the Protein Data Bank PDB [38]. Protein preparation was done using Schrödinger's Protein Preparation Wizard [39] by adding hydrogen atoms, assigning protonation states, and minimising the protein. Ligands were prepared in MOE [40] from smiles in neutral form. Multiple low energy starting conformations were generated with MOE within an energy window of 5 kcal/mol. Molecular docking was performed using program Glide software [39]. The same protocol was used as in a previous study [34]. Two conserved water molecules were included in the protein models, the best docking pose was selected based on the Glide SP score. All compounds were docked in neutral form.

In our previous study we found that rescoring the docking poses by using a MM-GB/SA protocol resulted in a significant correlation between calculated interaction energies and *in vitro* inhibition data. Therefore, the same protocol was applied to the compounds under study. To calculate binding free energy, we used the AMBER12EHT force field implemented in the MOE program together with the continuum solvation model GB/SA. The experimentally observed geometries of the zinc complexes were best reproduced using this setup. Partial charges were fixed using the MOE Protonate3D tool according to the used force-field followed by a short minimisation. An in-house script for minimising the protein–ligand complex and calculating the binding free energy was applied for all docking poses of ligands. During complex minimisation heavy atoms of protein were tethered with a deviation of 0.5 Å (force constant (3/2) $kT/(0.5)^2$).

The authors thank the COST action CM1406 (Epigenetic Chemical Biology EPICHEMBIO) for support. This work and the authors of this article received funding from the European Union's Seventh Framework Programme for Research, Technological Development and Demonstration under Grant Agreements 241865 (SEtTReND) and 602080 (A-ParaDDisE). We thank Karin Schmidtkunz for technical assistance. The work of J. L. and R. P. was also supported by institutional funds from the CNRS, the Institut Pasteur de Lille and the Université de Lille.

The authors have declared no conflicts of interest.

References

[1] World Health Organization, *Wkly. Epidemiol. Rec.* **2015**, *90*, 25–32 and schistosomiasis fact sheet; Available from: http://www.who.int/mediacentre/factsheets/fs115/en [accessed 08.12.16].
[2] F. Mutapi, *Pediatrics* **2015**, *135*, 536–544.
[3] M. Brown, *Schistosomiasis, Clin. Med. (Lond)* **2011**, *11*, 479–482.
[4] B. Gryseels, K. Polman, J. Clerinx, L. Kestens, Human schistosomiasis, *Lancet* **2006**, *368*, 1106–1118.
[5] M. Berriman, B. J. Haas, P. T. LoVerde, R. A. Wilson, G. P. Dillon, G. C. Cerqueira, S. T. Mashiyama, B. Al-Lazikani, L. F. Andrade, P. D. Ashton, M. A. Aslett, D. C. Bartholomeu, G. Blandin, C. R. Caffrey, A. Coghlan, R. Coulson, T. A. Day, A. Delcher, R. DeMarco, A. Djikeng, T. Eyre, J. A. Gamble, E. Ghedin, Y. Gu, C. Hertz-Fowler, H. Hirai, Y. Hirai, R. Houston, A. Ivens, D. A. Johnston, D. Lacerda, C. D. Macedo, P. McVeigh, Z. Ning, G. Oliveira, J. P. Overington, J. Parkhill, M. Pertea, R. J. Pierce, A. V. Protasio, M. A. Quail, M. A. Rajandream, J. Rogers, M. Sajid, S. L. Salzberg, M. Stanke, A. R. Tivey, O. White, D. L. Williams, J. Wortman, W. Wu, M. Zamanian, A. Zerlotini, C. M. Fraser-Liggett, B. G. Barrell, N. M. El-Sayed, *Nature* **2009**, *460*, 352–358.
[6] R. J. Pierce, F. Dubois-Abdesselem, S. Caby, J. Trolet, J. Lancelot, F. Oger, N. Bertheaume, E. Roger, *Mem. Inst. Oswaldo Cruz* **2011**, *106*, 794–801.
[7] A. A. Siddiqui, B. A. Siddiqui, L. Ganley-Leal, *Hum. Vaccin.* **2011**, *7*, 1192–1197.
[8] D. Cioli, L. Pica-Mattoccia, A. Basso, A. Guidi, *Mol. Biochem. Parasitol.* **2014**, *195*, 23–29.
[9] M. J. Doenhoff, J. R. Kusel, G. C. Coles, D. Cioli, *Trans. R. Soc. Trop. Med. Hyg.* **2002**, *96*, 465–469.
[10] M. J. Doenhoff, L. Pica-Mattoccia, *Expert Rev. Anti-Infect. Ther.* **2006**, *4*, 199–210.
[11] D. Alonso, J. Munoz, J. Gascon, M. E. Valls, M. Corachan, *Am. J. Trop. Med. Hyg.* **2006**, *74*, 342–344.
[12] I. M. Silva, R. Thiengo, M. J. Conceicao, L. Rey, H. L. Lenzi, E. Pereira Filho, P. C. Ribeiro, *Mem. Inst. Oswaldo Cruz* **2005**, *100*, 445–449.
[13] P. G. Fallon, M. J. Doenhoff, *Am. J. Trop. Med. Hyg.* **1994**, *51*, 83–88.
[14] F. F. Couto, P. M. Coelho, N. Araujo, J. R. Kusel, N. Katz, L. K. Jannotti-Passos, A. C. Mattos, *Mem. Inst. Oswaldo Cruz* **2011**, *106*, 153–157.
[15] S. M. Messerli, R. S. Kasinathan, W. Morgan, S. Spranger, R. M. Greenberg, *Mol. Biochem. Parasitol.* **2009**, *167*, 54–59.
[16] U. E. Martinez-Outschoorn, R. G. Pestell, A. Howell, M. L. Tykocinski, F. Nagajyothi, F. S. Machado, H. B. Tanowitz, F. Sotgia, M. P. Lisanti, *Cell Cycle* **2011**, *10*, 4208–4216.
[17] S. R. Choi, A. Pradhan, N. L. Hammond, A. G. Chittiboyina, B. L. Tekwani, M. A. Avery, *J. Med. Chem.* **2007**, *50*, 3841–3850.
[18] F. Hirschhaeuser, U. G. Sattler, W. Mueller-Klieser, *Cancer Res.* **2011**, *71*, 6921–6925.
[19] T. A. Rasmussen, O. Schmeltz Sogaard, C. Brinkmann, F. Wightman, S. R. Lewin, J. Melchjorsen, C. Dinarello,

L. Ostergaard, M. Tolstrup, *Hum. Vaccin. Immunother* **2013**, *9*, 993–1001.
[20] K. J. Falkenberg, R. W. Johnstone, *Nat. Rev. Drug Discov*. **2014**, *13*, 673–691.
[21] F. K. Hansen, S. D. Sumanadasa, K. Stenzel, S. Duffy, S. Meister, L. Marek, R. Schmetter, K. Kuna, A. Hamacher, B. Mordmuller, M. U. Kassack, E. A. Winzeler, V. M. Avery, K. T. Andrews, T. Kurz, *Eur. J. Med. Chem*. **2014**, *82*, 204–213.
[22] T. Harada, T. Hideshima, K. C. Anderson, *Int. J. Hematol*. **2016**, *104*, 300–309.
[23] R. Benedetti, M. Conte, L. Altucci, *Antioxid. Redox Signal*. **2015**, *23*, 99–126.
[24] J. A. Engel, A. J. Jones, V. M. Avery, S. D. Sumanadasa, S. S. Ng, D. P. Fairlie, T. S. Adams, K. T. Andrews, *Int. J. Parasitol. Drugs Drug Resist*. **2015**, *5*, 117–126.
[25] C. Dissous, C. G. Grevelding, *Trends Parasitol*. **2011**, *27*, 59–66.
[26] M. Marek, G. Oliveira, R. J. Pierce, M. Jung, W. Sippl, C. Romier, *Future Med. Chem*. **2015**, *7*, 783–800.
[27] F. K. Hansen, T. S. Skinner-Adams, S. Duffy, L. Marek, S. D. Sumanadasa, K. Kuna, J. Held, V. M. Avery, K. T. Andrews, T. Kurz, *ChemMedChem* **2014**, *9*, 665–670.
[28] F. Oger, F. Dubois, S. Caby, C. Noel, J. Cornette, B. Bertin, M. Capron, R. J. Pierce, *Biochem. Biophys. Res. Commun*. **2008**, *377*, 1079–1084.
[29] F. Dubois, S. Caby, F. Oger, C. Cosseau, M. Capron, C. Grunau, C. Dissous, R. J. Pierce, *Mol. Biochem. Parasitol*. **2009**, *168*, 7–15.
[30] J. Lancelot, S. Caby, F. Dubois-Abdesselem, M. Vanderstraete, J. Trolet, G. Oliveira, F. Bracher, M. Jung, R. J. Pierce, *PLoS Negl. Trop. Dis*. **2013**, *7*, e2428.
[31] M. Marek, S. Kannan, A. T. Hauser, M. Moraes Mourao, S. Caby, V. Cura, D. A. Stolfa, K. Schmidtkunz, J. Lancelot, L. Andrade, J. P. Renaud, G. Oliveira, W. Sippl, M. Jung, J. Cavarelli, R. J. Pierce, C. Romier, *PLoS Pathog*. **2013**, *9*, e1003645.
[32] A. Chakrabarti, I. Oehme, O. Witt, G. Oliveira, W. Sippl, C. Romier, R. J. Pierce, M. Jung, *Trends Pharmacol. Sci*. **2015**, *36*, 481–492.
[33] D. A. Stolfa, M. Marek, J. Lancelot, A. T. Hauser, A. Walter, E. Leproult, J. Melesina, T. Rumpf, J. M. Wurtz, J. Cavarelli, W. Sippl, R. J. Pierce, C. Romier, M. Jung, *J. Mol. Biol*. **2014**, *426*, 3442–3453.
[34] T. Heimburg, A. Chakrabarti, J. Lancelot, M. Marek, J. Melesina, A. T. Hauser, T. B. Shaik, S. Duclaud, D. Robaa, F. Erdmann, M. Schmidt, C. Romier, R. J. Pierce, M. Jung, W. Sippl, *J. Med. Chem*. **2016**, *59*, 2423–2435.
[35] L. Marek, A. Hamacher, F. K. Hansen, K. Kuna, H. Gohlke, M. U. Kassack, T. Kurz, *J. Med. Chem*. **2013**, *56*, 427–436.
[36] B. Heltweg, F. Dequiedt, E. Verdin, M. Jung, *Anal. Biochem*. **2003**, *319*, 42–48.
[37] B. Heltweg, F. Dequiedt, B. L. Marshall, C. Brauch, M. Yoshida, N. Nishino, E. Verdin, M. Jung, *J. Med. Chem*. **2004**, *47*, 5235–5243.
[38] H. M. Berman, J. Westbrook, Z. Feng, G. Gilliland, T. N. Bhat, H. Weissig, I. N. Shindyalov, P. E. Bourne, The Protein Data Bank, *Nucleic Acids Res*. **2000**, *28*, 235–242.
[39] S. Schrödinger Suite 2012 Protein Preparation Wizard; Epik Version 2.3, Schrödinger, Llc, New York, NY, 2012; Impact Version 5.8, Schrödinger, Llc, New York, NY, 2012; Prime Version 3.1, Schrödinger, Llc, New York, NY, 2012.
[40] Molecular Operating Environment (Moe), 2012. 10; Chemical Computing Group Inc., 1010 Sherbooke St. West, Suite #910, Montreal, Qc, Canada, H3a 2r7, 2012.